Materials Science and Engineering A 527 (2010) 1776–1783

Contents lists available at ScienceDirect

Materials Science and Engineering A

journal homepage: www.elsevier.com/locate/msea

Grain refinement and mechanical properties in ultrafine grained Pd and Pd–Ag alloys produced by HPT

L. Kurmanaeva[a,*], Yu. Ivanisenko[a], J. Markmann[a,b], C. Kübel[a], A. Chuvilin[c], S. Doyle[d], R.Z. Valiev[e], H.-J. Fecht[a,f]

[a] Institute für Nanotechnologie, Karlsruhe Institute für Technologie, Hermann-von-Helmholtz-Platz 1, 76344 Eggenstein-Leopoldshafen, Germany
[b] Universität des Saarlandes, FR7.3 Technische Physik, Campus D2 2, 66123 Saarbrücken, Germany
[c] Materialwissenschaftliche Elektronenmikroskopie, Universität Ulm, Albert-Einstein-Allee 11, 89081 Ulm, Germany
[d] Institut für Synchrotronstrahlung, Karlsruhe Institute of Technologie, PO Box 3640, 76021 Karlsruhe, Germany
[e] Institut of Physics of Advanced Materials, Ufa State Aviation Technical University, K.Marx 12, 450000 Ufa, Russia
[f] Institut für Mikro- und Nanomaterialien, Universität Ulm, Albert-Einstein-Allee 47, 89081 Ulm, Germany

ARTICLE INFO

Article history:
Received 13 August 2009
Received in revised form 30 October 2009
Accepted 2 November 2009

Keywords:
Palladium alloys
High pressure torsion
Ultrafine grained materials
Stacking fault energy
Strain hardening behaviour

ABSTRACT

The microstructure and the mechanical properties of ultrafine grained Pd and Pd–*x*% Ag ($x = 10, 20, 40$) alloys processed by high pressure torsion (HPT) were thoroughly investigated using transmission and high resolution electron microscopy, XRD analysis and tensile tests. The increased Ag content resulted in decrease of the stacking fault energy (γ_{SF}), which made it possible to produce by means of HPT different ultrafine-grained structures in the alloys and to study their superior strength and ductility. The nature of such unique mechanical behaviour is discussed on the basis of analysis of strain hardening mechanisms and effect of stacking fault energy.

1. Introduction

In the past, a strong progress has developed in severe plastic deformation (SPD) techniques [1,2]. It has become possible to produce ultrafine grained (UFG) materials in commercially reasonable amounts. Thanks to their outstanding mechanical properties UFG materials obtained by means of SPD offer a wide range of applications as structural building units and components. The potential for technical innovations based on SPD materials has been demonstrated for many areas [3,4], e.g. production of medical implants fabricated from commercially pure Ti processed by SPD [5].

It is common knowledge that UFG materials exhibit superior hardness, strength and fatigue properties as compared to their coarse grained counterparts. However, often they possess a lack of ductility or are affected by rapid strain localization. Usually, stress–strain curves of these materials show failure immediately after onset of yielding [6]. Such behaviour is related to the low strain hardening capacity of UFG materials due to limited dislocation storage in small grains. It is expected that any improvement of strain hardening will be beneficial for the ductility, i.e. enhancing the uniform elongation, in UFG materials [7].

Several routes to improve the ductility of UFG materials were suggested, such as generating bimodal grain size distributions, nano-twins, and dispersion of nano-particles [8]. A quite current method is to increase the ductility by alloying with specific materials with the purpose of decreasing the stacking fault energy (γ_{SF}) as shown in Refs. [9,10].

The objective of this study was to investigate the deformation behaviour and the microstructure in UFG Pd–Ag alloys processed by high pressure torsion. Addition of Ag dramatically decreases γ_{SF} in Pd–Ag alloys. It was demonstrated that alloying leads to improvement of both strength and ductility in these alloys. This effect is explained by the enhanced strain hardening capacity thanks to the UFG microstructure with high density of pre-existing dislocations formed as a result of HPT. Such microstructure not only provides a significant increase of the yield strength as compared to pure Pd, but it also helps to sustain further straining due to the enhanced hardening rate.

* Corresponding author at: Institute für Nanotechnologie, Karlsruhe Institute für Technologie, Hermann-von-Helmholtz-Platz 1, 76344 Eggenstein-Leopoldshafen, Germany. Tel.: +49 7247 82 6450; fax: +49 7247 82 8298.
E-mail address: lilia.kurmanaeva@kit.edu (L. Kurmanaeva).

0921-5093/$ – see front matter © 2009 Elsevier B.V. All rights reserved.
doi:10.1016/j.msea.2009.11.001

Table 1
Physical properties: melting temperature (T_m) [10], elastic shear modulus (G) [11], stacking fault energy (γ_{SF}) [12] and initial microhardness of studied alloys.

% Ag	T_m, °C	G, GPa	γ_{SF}, mJ/m^2	Initial microhardness, HV
0	1555	46.2	179	42 ± 5
10	1510	44.5[a]	165.3	45 ± 4
20	1470	42.8[a]	125	66 ± 10
40	1385	39.5[a]	118.7	62 ± 8

[a] Shear module of Pd–Ag alloys was estimated from E of pure Pd and Ag using the rule of mixture.

2. Experimental materials and procedures

Pd and Pd–x% Ag (x = 10, 20, 40) samples were alloyed by heating and melting in an arc-melting oven under Ar atmosphere. According to the phase diagram Pd and Ag are completely soluble [11]. The physical properties (melting temperature [11], elastic shear modulus [12], stacking fault energy [13]) and the initial microhardness of the investigated materials are presented in Table 1. The stacking fault energy of Ag (22 mJ/m^2) is significantly lower than that of Pd (169 mJ/m^2) [13], hence the addition of Ag decreases γ_{SF} in Pd–Ag alloys (Table 1). The ingots were processed by HPT under quasi-hydrostatic pressure of 6 GPa for five rotations, description of this SPD technique is published elsewhere [1]. The final dimensions of the HPT-disks were about 10 mm in diameter and 0.3 mm in thickness.

Initial microhardness of studied samples was measured with a microindenter (Bühler^{TM}) at a load of 2 N. At least 5 indents were averaged for each data.

Tensile specimens were cut out of HPT-disks as shown in Fig. 1a and thereafter mechanically fine polished using diamond suspensions with particle size down to 3 μm. Uniaxial tensile tests were performed at room temperature using a dedicated tensile stage for miniature specimens at a strain rate of 10^{-3} s^{-1}. The elongation was precisely measured using a laser extensometer P-50 by Fiedler Optoelectronics to read TiO_2 marks that had been applied on the tensile specimens' surfaces as shown in Fig. 1b. At least three tensile samples were used for each condition to obtain statistically valid results.

Transmission electron microscopy (TEM) investigations were performed using a Philips CM-30 operated at 300 kV, and high resolution transmission electron microscopy (HRTEM) studies were performed using a FEI Titan 80-300 with imaging C_S-correction (FEI, Netherlands). Specimens for TEM were taken from a location corresponding to the gauge section of the tensile specimen and situated

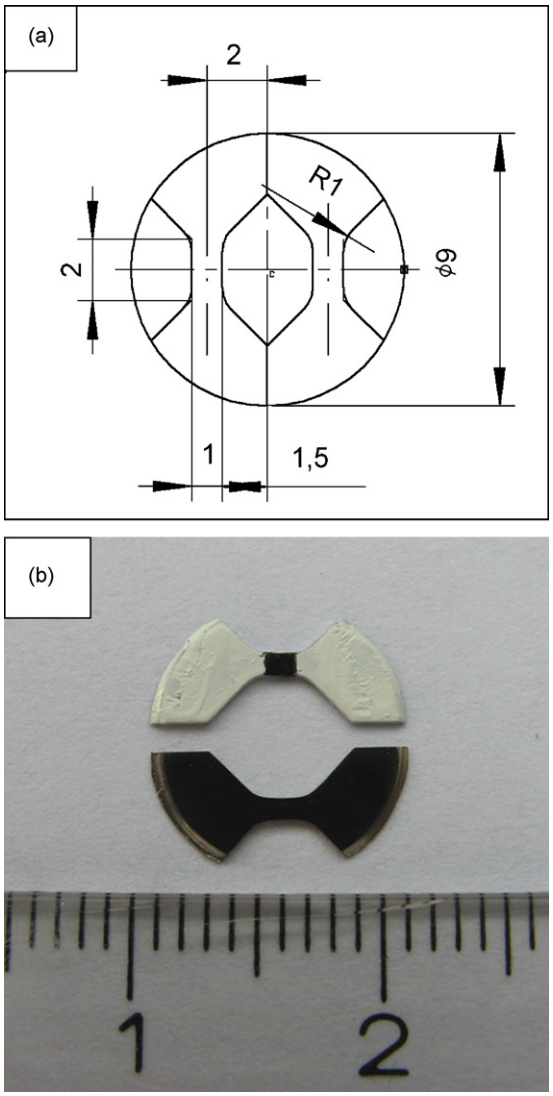

Fig. 1. Tensile specimens: (a) schematic representation showing cutting position of tensile specimens in HPT-disks. (b) View of the specimens before tensile test.

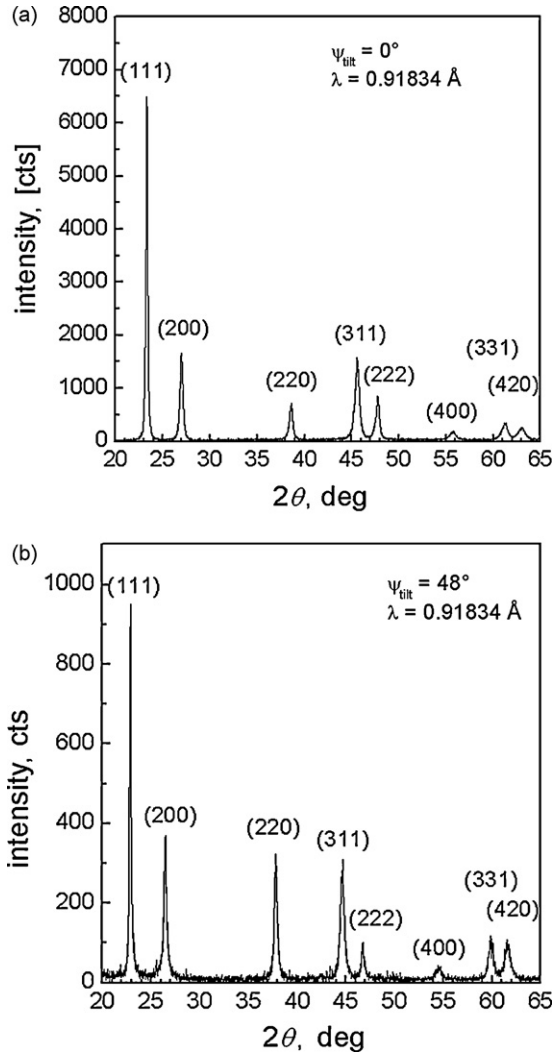

Fig. 2. X-ray diffractograms of HPT-processed Pd, measured in specimen plane view at $\Psi = 0°$ (a) and $\Psi = 48°$ (b). Samples were processed by HPT under quasi-hydrostatic pressure of 6 GPa for five rotations. The XRD measurements were conducted in the sample areas situated at a distance of 3 mm from the sample centre.

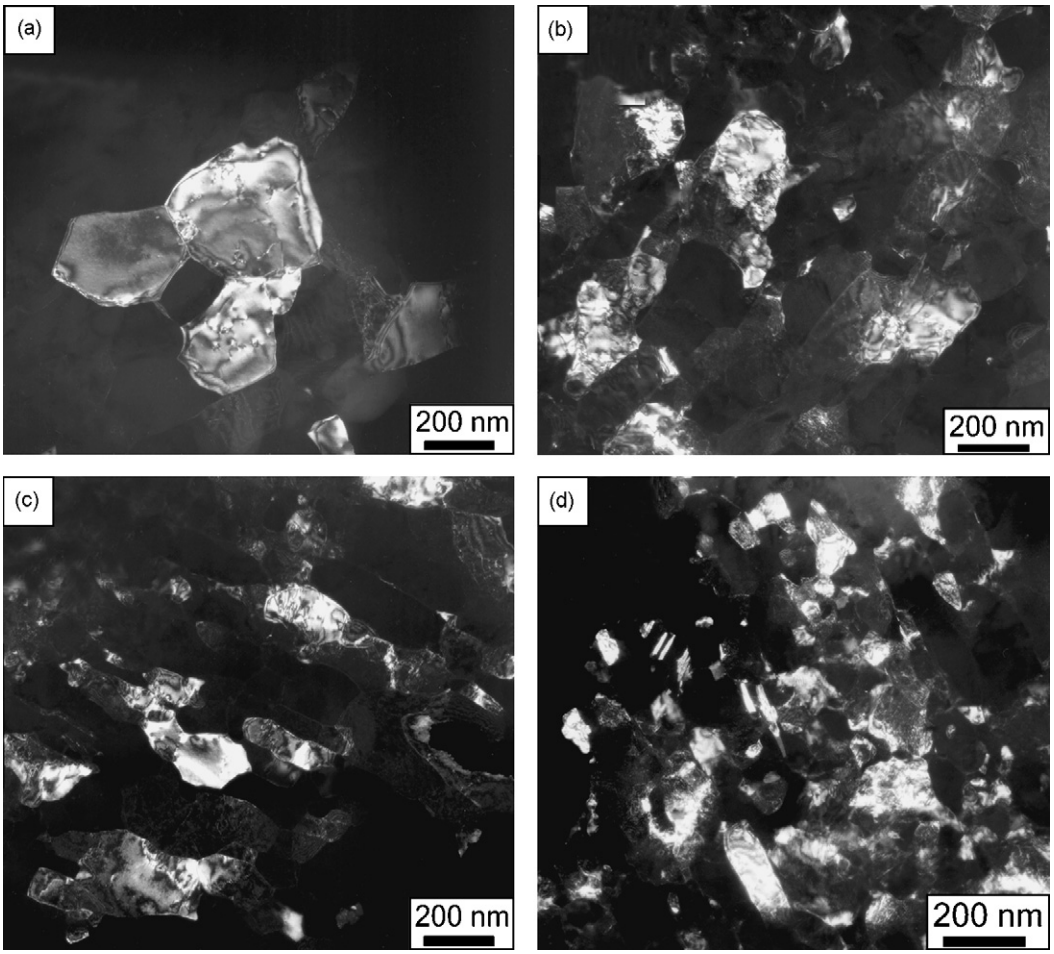

Fig. 3. TEM dark-field images of typical microstructures taken in a plane view of HPT-processed Pd (a), Pd–10% Ag (b), Pd–20% Ag (c), and Pd–40% Ag (d). Samples were processed by HPT under quasi-hydrostatic pressure of 6 GPa for five rotations. The microstructure investigations were conducted in the sample areas situated at a distance of 3 mm from the sample centre.

at a distance of 3 mm from the sample centre. TEM specimens of Pd were prepared by electropolishing using a Tenupol 5 electropolishing apparatus (Struers A/S, Denmark) with a BK-2 electrolyte [14] at −20 °C. For the preparation of thin foils of Pd–Ag alloys a two step procedure was applied. They were mechanically grinded and dimpled, and then further thinned to a thickness of electron transparency using a Gatan Precision Ion Polishing System (PIPS, Gatan, USA) with an Ar^+ ions accelerated at 2.5–3.5 kV. In order to remove the ion damaged layer from the thin foil surfaces, further electropolishing with an electrolyte consisting of methyl alcohol (6 volumes), nitric acid (4 volumes), and phosphoric acid (2 volumes) at a temperature of −15 °C and at voltage of 22 V was applied. The mean grain size was estimated using a line interception method [15] in representative dark field TEM images. The line interceptions were measured in two directions: in the direction of shear deformation during HPT, and perpendicular to it. The final grain size was calculated as the average between length and width. For a statistical distribution of the grain sizes a total of 150–200 grains were measured for each analysis.

3. Synchrotron XRD measurements with a correction for residual stresses

Quantitative XRD measurements of the HPT-processed samples were performed using the synchrotron ANKA at the Research Center Karlsruhe. The XRD measurements were conducted in the sample areas situated at a distance of 3 mm from the sample centre. The beam diameter was 1 mm. The peak profile parameters (peak intensity, full width at half maximum and integral breadth) were determined by fitting a Pearson VII function to the measured peaks. The volume averaged crystallite size and the microstrain were estimated from the XRD peak broadening using a modified Williamson–Hall method correcting for systematic errors as described in Ref. [16]. All reflections with Miller indices up to (4 2 0) were used for the grain size and microstrains estimates. A LaB_6 standard by NIST was used to determine the correction for instrumental broadening. For evaluation of the lattice parameters (a) and stacking fault probabilities (α_{SF}) [17], a special route of correction for residual stresses was performed. This procedure was necessary because HPT deformation is characterized by very high residual stresses in the processed specimens. Residual stresses cause shifts of XRD peaks, and consequently, may affect the results of the estimation of the lattice parameter or stacking fault probability out of peak positions and peak shifts. It was shown, that a tilting of the sample with respect to the XRD diffraction plane at a certain angle (angle Ψ in a standard Eulerian coordinate system), the influence of the residual stresses on the position of a certain XRD peak can be eliminated [18]. For Pd these tilt angles are quite similar for all crystallographic directions at about 48° (see Ref. [18] for details). Therefore the synchrotron XRD measurements used for the determination of the lattice parameter and the stacking fault density were performed at this angle using an Eule-

Table 2
Results of quantification of microstructural details of HPT-processed Pd and Pd–Ag alloys: TEM grain size (d), XRD crystallite size ($\langle X \rangle$), microstrain ($\langle \varepsilon^2 \rangle^{1/2}$), stacking fault probability (α_{SF}), dislocation density (ρ) and lattice parameter (a).

% Ag	d, nm	$\langle X \rangle$, nm	$\langle \varepsilon^2 \rangle^{1/2}$, %	α_{SF},%	$\rho \times 10^{15}$, m^{-2}	a, pm
0	240 ± 15	86.45 ± 6.35	0.06 ± 0.01	0.055	0.07	389.04 ± 0.01
10	206 ± 11	50.7 ± 5.0	0.26 ± 0.01	0.34	1.4	389.98 ± 0.09
20	150 ± 15	29.8 ± 2.2	0.37 ± 0.01	0.82	2.8	392.69 ± 0.19
40	144 ± 14	23.55 ± 1.65	0.30 ± 0.02	0.27	1.8	395.85 ± 0.05

rian cradle. X-ray diffractograms measured with correction and without it for pure Pd are presented in Fig. 2. Anticipating results of this experiment, and taking pure Pd as the example, we note that the values of lattice parameter estimated using the measurements conducted at $\Psi = 0^\circ$ and $\Psi = 48^\circ$ were 389.124 ± 0.045 pm and 389.041 ± 0.008 pm, respectively. It is clearly seen, that residual stress leads to a notable overestimate of the lattice parameter, whereas lattice parameter measured using $\Psi = 48^\circ$ is very close to that of as-cast material (389.056 ± 0.012 pm).

As residual stress does not influence the estimate of the volume averaged crystallite size and the average amount of microstrain, these values were estimated using the X-ray diffractograms measured at $\Psi = 0^\circ$.

4. Results

4.1. Microstructure of Pd–Ag alloys resulting from HPT

Fig. 2 shows typical dark-field images of as-HPT-processed Pd and Pd–Ag alloys. The microstructure of all samples is characterized by slightly elongated grains with an aspect ratio of about 1.5. It is also shown that alloying leads to a decrease of the resulting grain size (Fig. 3a–d).

The mean grain size in as-HPT Pd is 240(15) nm as determined by TEM. Grains are delineated by narrow and distinct grain boundaries as shown in Fig. 3a. Separate dislocations and dislocation subboundaries (note the considerably smaller grain size as esti-

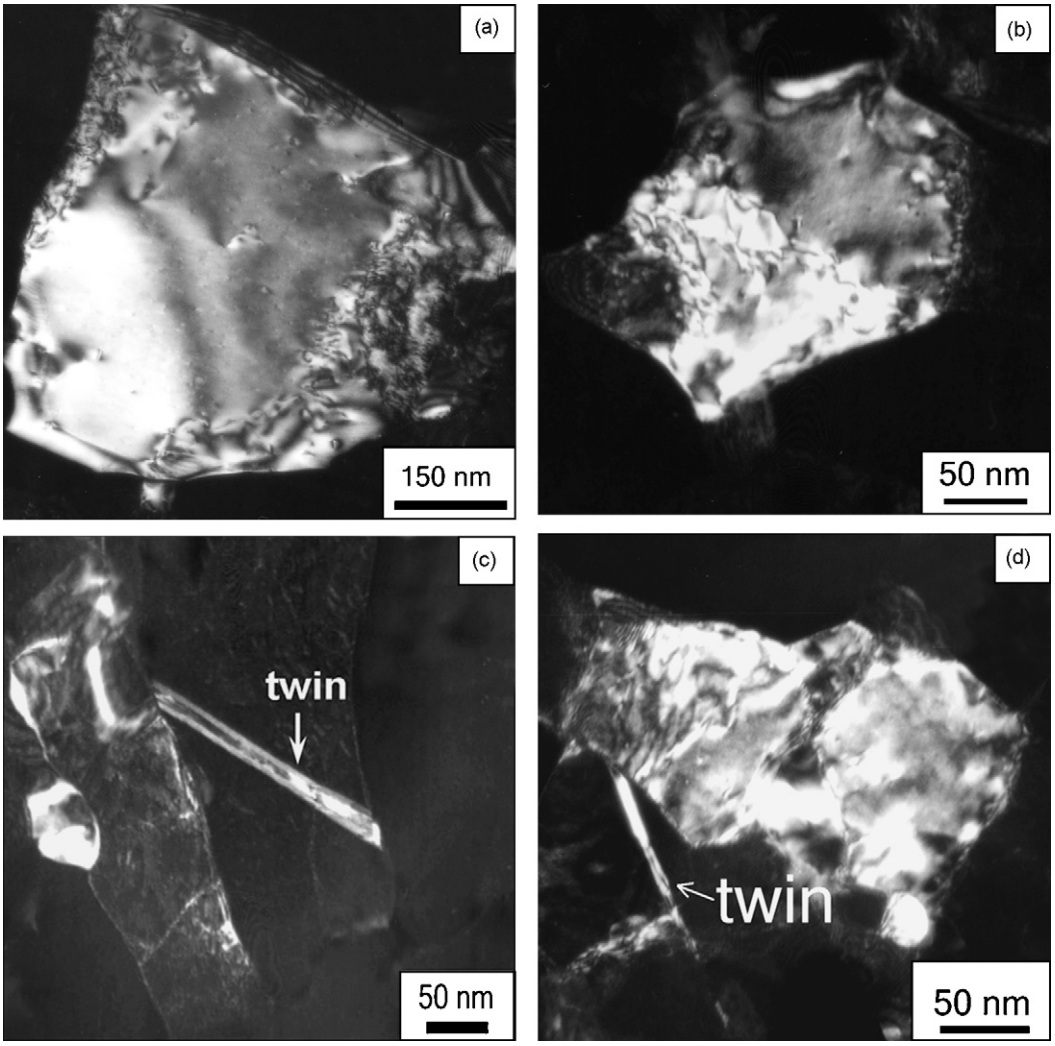

Fig. 4. Plane view TEM dark-field images showing defect structures in HPT-processed Pd (a), Pd–20% Ag (b and c) and Pd–40% Ag (d). Samples were processed by HPT under quasi-hydrostatic pressure of 6 GPa for five rotations. The microstructure investigations were conducted in the sample areas situated at a distance of 3 mm from the sample centre.

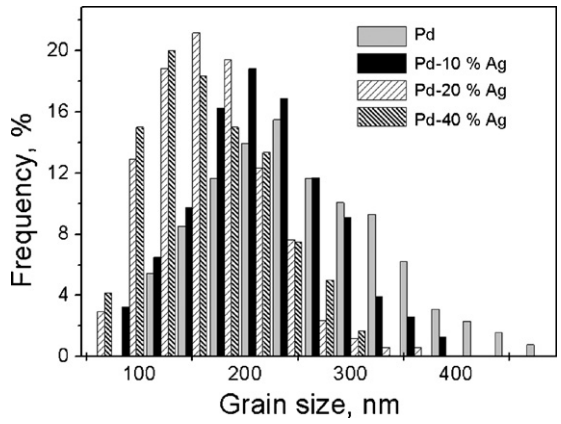

Fig. 5. Grain size distribution in HPT-processed Pd, Pd–10% Ag, Pd–20% Ag and Pd–40% Ag (before tensile tests).

mated by XRD, see Table 2) are observed inside the grains (Fig. 4a). The microstructure of as-HPT alloys looks different as compared to that of pure Pd. The grain size becomes notably smaller, e.g. the mean grain size in the Pd–10% Ag and Pd–20% Ag is 206(11) and 150(15) nm, respectively (Fig. 3b and c), and dense dislocation tangles and pile ups are present in all grains (Fig. 4b). Additionally, in the Pd–20% Ag very narrow nano-twins with a thickness of several nm can be found in some grains (Fig. 4c). Further increase of the Ag content leads to a further decrease of the resulting grain size to 144(15) nm in the Pd–40% Ag alloy (Fig. 3d). Upon that, the number of grains with nano-twins visually increases, and the dislocation density inside the grains is still high (Fig. 4d).

The statistical analysis of the grain size distributions determined from dark field TEM images is shown in Fig. 5. It is evident that the width of the grain size distribution is reduced with increasing Ag content, thereby demonstrating that the microstructure becomes more uniform.

Additionally, the following microstructure parameters like the volume averaged crystallite size, the average amount of microstrain, the lattice parameter, and the stacking fault probability were evaluated from the analysis of the XRD peak profiles obtained using synchrotron radiation, and the results are summarized in Table 2. Similar to the TEM observations, the XRD crystallite size is also decreasing with increasing Ag content. Furthermore, both the microstrain and the stacking fault probability α_{SF} are increasing with increasing Ag content (Table 2).

4.2. HRTEM observations of stacking faults in Pd–20% Ag alloy

The high values of α_{SF} for Pd–20% Ag (Table 2) indicate that dislocations are very likely to split. However, the splitting distance is not large enough to be distinguished from unsplit dislocations in conventional TEM images. Indeed, HRTEM observations in [1 1 0] orientation revealed numerous staking faults (SFs) (Fig. 6, inserts A and B) and staking faults tetrahedrons (Fig. 6, insert C). The stacking faults lay in the (1 1 1) crystallographic planes. We measured the widths of 50 SF ribbons from HRTEM images. They span a range from 3 to 5.5 nm with an average width of 4.4 nm. The SFs in Fig. 6A are shown edge on. A Burgers circuit [19] has been drawn showing a closing failure due to the presence of a Shockley partial dislocation as indicated. Very often, however, the lattice shift across the apparent SF line appears unclear (Fig. 6, insert B), but the stress field related with the SF straightforwardly reveals its presence. We should emphasize that a high local density of stacking faults was revealed in our HRTEM observations. Typically, 10–15 SFs can be seen simultaneously in a field of view (area 35 nm × 35 nm). On the other hand, areas free of any defects can also be observed in HRTEM.

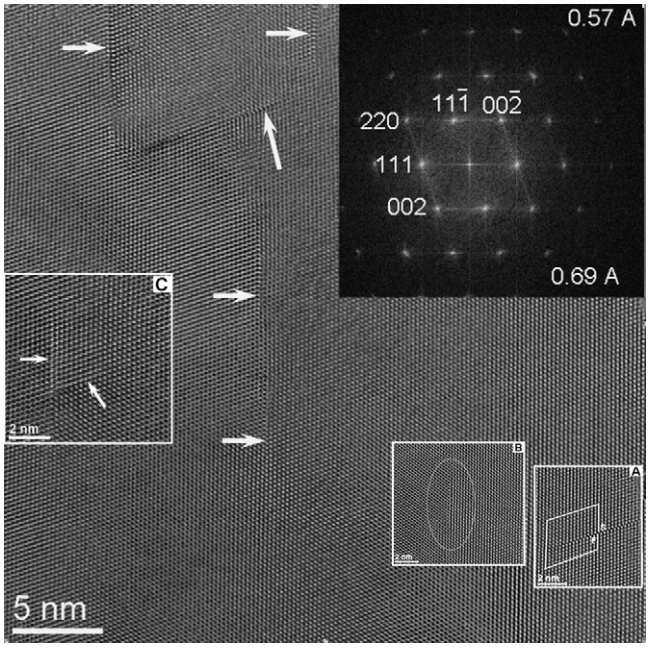

Fig. 6. HRTEM image of stacking faults in HPT-processed Pd–20% Ag viewed along ⟨1 1 0⟩, insert shows corresponding FFT. Several SFs are indicated with arrows, and two defects are shown enlarged in A and B: in A lattice shift in $11\bar{1}$ is clearly seen as shown by a Burgers circuit; S refers to the starting point and F the finishing point of the Burgers circuit, respectively; in B stacking fault is indicated by oval, lattice shift is not so clearly seen as in A. C Shows stacking fault tetrahedron.

4.3. Mechanical properties

Fig. 7a shows the typical tensile curves of the UFG Pd, Pd–10% Ag, Pd–20% Ag, and Pd–40% Ag alloys. It is apparent that the strength of the materials studied is increasing with increasing Ag content. Remarkably, the Pd–20% Ag and the Pd–40% Ag alloys did not only show the highest values of yield and ultimate strength, but also the largest uniform strain (Table 3). Fig. 7b shows the normalized strain hardening rate (Θ) versus true stress calculated as:

$$\Theta = \frac{d\sigma}{d\varepsilon}, \quad (1)$$

where σ denotes the true stress and ε the logarithmic strain. Only segments of the tensile curves in Fig. 7a corresponding to the uniform elongation of the sample (i.e. between open squares and open circles) were used for the calculation of Θ. It proves that Θ increases with the increase of the Ag content higher than 20%.

5. Discussion

5.1. Microstructure evolution

The microstructures that developed as a result of severe plastic deformation by HPT in pure Pd and in all studied Pd–Ag alloys varied with respect of both the grain size and the defect substructure. The increase of Ag content led to a decreasing grain size, an increase of the dislocation density, and a formation of stacking faults and twins.

Table 3
List of mechanical properties: yield stress (YS), ultimate stress (UTS), uniform strain (ε_u), fracture strain (ε_f) and area reduction in the neck (ψ) of HPT samples.

% Ag	YS, MPa	UTS, MPa	ε_u, %	ε_e, %	ψ, %
0	628 ± 5	760 ± 25	0.035 ± 0.002	0.16 ± 0.005	53
10	870 ± 10	1153 ± 15	0.05 ± 0.003	0.16 ± 0.003	37
20	975 ± 12	1215 ± 20	0.055 ± 0.002	0.135 ± 0.007	32
40	1000 ± 5	1130 ± 10	0.055 ± 0.002	0.15 ± 0.005	32

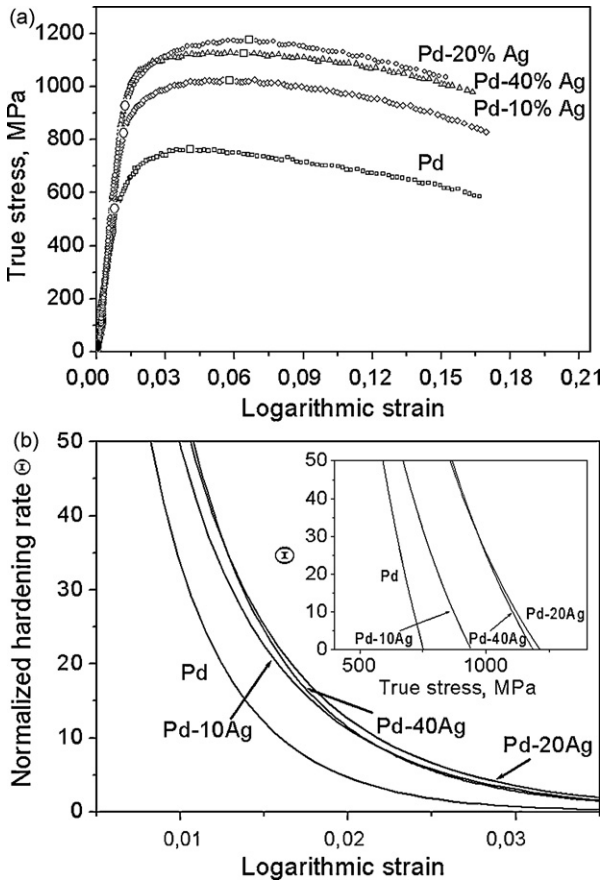

Fig. 7. (a) Tensile stress–strain curves of UFG Pd, Pd–10% Ag, Pd–20% Ag Pd–40% Ag. The circles indicate the onset of yielding and the squares point to the ultimate stress. Strain was measured by means of the laser extensometer. (b) Normalized work hardening rate θ against strain and stress.

In the following sections we are going to discuss these features separately.

5.1.1. Grain refinement on HPT

Alloying with Ag significantly influences the grain size resulting from HPT: the larger the Ag content, the smaller the grain size.

It is well accepted [1,20–22] that the microstructural evolution during HPT occurs as a sequence of several steps (or stages) and begins with the formation of a cell structure with high dislocation density located in the cell boundaries. When the HPT straining is continued over a wide range of strains a non-homogenous microstructure is formed with a broad grain size and grain orientation distribution. However, the mean grain/cell size gradually decreases with increasing strain and the permanent storage of dislocations in cell boundaries leads to an increase of their misorientations. Finally, a steady stage is reached where the mean grain size achieves the lowest value, and neither the mean grain size nor the grain boundary misorientation distribution can be influenced by further deformation [1,20]. The occurrence of a steady state grain size is also typical for ball milling [21], but the grain size achieved at ball milling is usually lower than that after high pressure torsion. The physical reason for establishing the steady stage is not quite clear yet; it was proposed that the lowest grain size results from the balance between the produced dislocations and their recovery by thermal processes [22]. Obviously, the number of produced dislocations depends on the accumulated strain and should be similar in different materials which experienced the same strain. Then the rate of dynamic recovery is the crucial parameter for the steady stage grain size. This model helps to understand the role of alloying in the process of grain refinement at HPT of Pd–Ag alloys. First of all, pinning of dislocations by solute atoms restricts their free path leading to the smaller cell size. Furthermore, the stacking fault energy decreases rapidly with increasing Ag content (Table 1). As our HRTEM investigation has shown (Fig. 6), smaller γ_{SF} in the Pd–20% Ag alloy leads to the dissociation of dislocations, which hinders cross-slip and climbing, and consequently, the ability of the material for a deformation recovery, which in its turn leads to an enhanced dislocation storage. Dislocation tangles may rearrange to new cell boundaries and movable dislocations readily sink to cell boundaries promoting their transformation to high angle boundaries [1]. The importance of γ_{SF} for the final grain size achieved after severe plastic deformation was shown for ball milling [23] and high pressure torsion [24–26]. In all cases the smaller the γ_{SF}, the smaller the resulting grain size.

According to Mohammed [23], other factors may influence the final grain size during severe plastic deformation. In particular, the higher the initial hardness, shear modulus, and melting temperature, the smaller will be the resulting grain size [23]. Despite all these parameters (except hardness) are decreasing in Pd–Ag alloys with increasing Ag concentration (Table 1), the resulting grain size has been decreasing, indicating that the stacking fault energy is a much more important parameter for grain refinement during SPD.

5.1.2. Dislocations, stacking faults, and twins

Our TEM investigations demonstrated a notable increase of dislocation density in the Pd–Ag alloys with increasing Ag content, despite the decreasing grain size. Analysis of the XRD peak profiles also revealed a concomitant increase of the microstrain (Table 2). Microstrain is related to the dislocation density by [27,28]:

$$\rho_{\text{strain}} = \frac{k\langle\varepsilon^2\rangle}{Fb^2}, \tag{2}$$

where ρ_{strain} is the dislocation density due to the microstrain and b the absolute of the Burgers vector, k depends on the kind of dislocations and the strain distribution due to their stress field and F describes their interaction. Quite elaborated methods exist in literature to determine the influence of the kind of dislocations on the strain broadening, especially the use of so-called contrast factors which describe the crystallographic anisotropy of the strain broadening and which do even allow for a distinction of the character of the dislocations (i.e. edge or screw) [29]. However, in the case of present study, the formula (2) should be sufficient because we just want to investigate the change of dislocation density as a function of the silver content. We took $F = 1$, i.e. we assume non-interacting dislocations in the grain interior while all interacting dislocations build up the cell boundaries and their influence on the X-ray peak broadening is considered as size broadening and therefore distinguishable by the size–strain separation of the Williamson–Hall analysis. A value of $k = 16$ as calculated by Williamson and Smallman describing the strain field of a screw dislocation in a fcc material [27] was used for the calculation of the dislocation densities.

In Table 2 the values of the dislocation density calculated using Eq. (2) for all studied alloys are presented. The dislocation density ρ increases almost linearly for 40 times from 0.07×10^{15} m^{-2} in pure as-HPT Pd to 2.8×10^{15} m^{-2} in the Pd–20% Ag alloy. Similar values were reported for HPT-processed Cu–Zn alloys, with the same trend for increasing ρ with decreasing stacking fault energy of the alloy [26]. As discussed above, the enhanced dislocation storage in alloys with higher Ag content is related to two factors: pinning of dislocations by solute atoms and splitting of dislocations promoted by lower γ_{SF}. In HRTEM images of the Pd–20% Ag alloy, we observed numerous SFs (Fig. 6) confirming dislocation splitting in agreement with the high stacking fault probability of 0.82% in this alloy (Table 2) as estimated by XRD. Nevertheless, further decreasing of

stacking fault energy in Pd–40% Ag did not lead to further increase of dislocation density, but to its decrease and surprisingly, also to drastic decrease of stacking fault probability (Table 2). Presumably, low γ_{SF} in Pd–40% Ag facilitates the development of deformation twinning (at the expense of the formation of stacking faults) which concurs with dislocation slip.

Another indication of the high activity of dissociated dislocations during severe plastic deformation is the observation of the SF tetrahedrons formation in the Pd–20% Ag alloy (Fig. 6, insert C). Such defects can be frequently found in metals and alloys with a low and medium γ_{SF} after cold deformation [26]. According to the mechanism suggested in Ref. [26], SF tetrahedrons can be formed by the glide of jogged screw split dislocations. Further mechanisms of SF tetrahedrons formation are discussed in Ref. [30].

5.2. Mechanical behaviour

When discussing the mechanical behaviour of UFG Pd and Pd–Ag alloys, one should keep in mind that tensile tests have been performed using miniature specimens with a gauge length as small as 1.4 mm. It is well known, that dimensions of the tensile specimens can influence the resulting mechanical properties, primarily the measured elongation. That is why dimensions of tensile specimens are fixed in corresponding standards [31]. The specimen sizes used in the present investigation do not meet these standards; therefore uniform and total elongations obtained cannot be compared with results of tensile tests performed using specimens having other dimensions. However, elongations of different samples within the present investigations can be readily compared to each other.

5.2.1. Enhanced strength.

The present studies demonstrated a significant increase of strength as a result of SPD for all studied alloys, with maximal values achieved in the Pd–20% Ag and Pd–40% Ag alloys (Table 3). Several factors contribute to this increase of the strength: small grain size, high dislocation density, and solute hardening. Obviously, the most important factor here is the grain size hardening according to the Hall–Petch relation [32,33] as $\sigma_{HP} \sim d^{-1/2}$. The smaller the grain size, the higher the strength, and consequently the highest values of the yield strength were obtained in alloys with the smallest grain size (Tables 2 and 3).

The next factor contributing to the enhanced strength is the strain hardening due to dislocation storage during plastic deformation. Already Taylor has shown that, if the influence of the dislocation density on the flow stress is dominant, then its contribution to flow stress is proportional to $\sqrt{\rho}$ [34]. Here we would like to stress that this is valid only for randomly distributed dislocations: dislocation forest. Our TEM and HRTEM observations show that number of randomly distributed dislocations in grain interior increases with alloying. Furthermore, Eq. (2) used for estimation of dislocation density from XRD data accounts only on distortions from non-interacting dislocations, and this density increases dramatically with increasing Ag content and achieves its maximum value in the Pd–20% Ag alloy (Table 2).

Solution hardening is much less important for strength of the HPT-processed Pd–Ag alloys. As it was mentioned before, the system Pd–Ag is completely soluble. The atomic radii of Pd and Ag are 137.6 pm and 144.4 pm, respectively. This difference in atomic diameters results only in a low solute hardening. A study performed on single crystals of Pd–Ag alloys demonstrated that in the concentration range up to 25 at.% Ag, the yield strength of alloys increases linearly with the increasing Ag concentration. Further increase of Ag leads to a (again linear) decrease of the yield strength [35]. Therefore the maximal hardening effect was achieved for a concentration of 25% of Ag and its value was only 20 MPa.

Hence, we conclude that the enhanced yield strength of HPT-processed Pd–20% Ag and Pd–40% Ag alloys results mainly from the smaller grain size and the increased dislocation density. Upon that slightly lower mean grain size in Pd–40% Ag, and slightly larger dislocation density in Pd–20% Ag lead to very close yield strength values in these alloys. Though, we admit that both factors are present simultaneously, it is very difficult to find out a quantitative correlation between the microstructural parameters and the flow stress, because existing theories do not describe their simultaneous influence.

5.2.2. Strain hardening behaviour

Usually UFG materials fail to exhibit a reasonable uniform elongation due to their limited strain hardening capacity. The strain hardening capacity reflects the ability of the material to store dislocations produced during plastic deformation, which is difficult in small grains because grain boundaries which can act as dislocation sinks are in direct vicinity. At a first glance we observe an unusual behaviour in the Pd–Ag alloys: the strain hardening capacity (SHC) and the highest uniform elongation was found in the Pd–20% Ag alloy, whereas the mean grain size in this alloy is almost 2 times smaller than that in pure Pd (Tables 2 and 3).

It is common knowledge, that the dislocation density in SPD materials is low, because dislocations usually sink into grain boundaries or self-organize into ordered substructures like cell and subgrain boundaries [1]. A typical example for this is represented by the microstructure of HPT-processed Pd (Figs. 3a and 4a). However, in the Pd–20% Ag and the Pd–40% Ag alloys dislocation tangles can be seen in all grains and the dislocation density is almost one order of magnitude higher comparing to that of pure Pd. As was discussed above, the enhanced dislocation storage is enabled by the lower γ_{SF} in the Pd–20% Ag and the Pd–40% Ag alloys compared to pure Pd which leads to a dislocation dissociation and impedes deformation recovery. Obviously, these pre-existing dislocations are not involved in the plastic flow during tensile testing, because otherwise stress–strain curves would demonstrate no or very low strain hardening which is not the case. On the other hand, pre-existing dislocations may provide sources for new dislocations, and act as barriers for dislocation glide (e.g. Peierls–Nabarro and Cottrell locks). The first provides the necessary source for dislocations, and the second hinders dislocations from sinking into the grain boundaries. The annihilation of dislocations is also retarded because cross-slip of split dislocations is difficult. Therefore, such an unique UFG microstructure with high density of pre-existing dislocations as formed in the Pd–Ag alloys as a result of HPT does not only provide a significant increase of the yield strength as compared to pure Pd, but it also helps to sustain further straining due to the enhanced hardening rate.

In the range of Ag content from 20 at.% till 40 at.% further decreasing of γ_{SF} and increasing of splitting distance of dislocations lead to transition of deformation mechanism from faulting to twinning. The transition is accompanied by a slight decrease of the dislocation density (Table 2) and increasing of the volume fraction of grains with nano-twins inside. It was shown by Zhao et al. [9,10] that formation of deformation nano-twins results in both more effective blockage of dislocation slip and in a larger amount of dislocation accumulation sites. Therefore in the concentration range of Ag between 20 and 40% we observe the interplay of two mechanisms of SHC improvement: one is based on the formation of stacking faults, and the second one on the formation of nano-twins. This interplay promotes the persistence of high mechanical properties in a wide concentration range.

6. Summary

(i) The ultrafine-grained structure formation during HPT in pure Pd and Pd–x% Ag (x = 10, 20, and 40) alloys has been investigated by means of synchrotron XRD analysis and TEM. It is shown that the addition of Ag leads to a decrease of the mean grain size from 240 nm in the pure Pd to 144 nm in the Pd–40% Ag mutually caused by the decreased stacking fault energy.

(ii) Tensile tests of the HPT-processed samples have demonstrated that alloying leads to improvement of both strength and ductility in UFG Pd–Ag alloys. In the concentration range of Ag between 20 and 40%, the yield strength is 975 MPa and 1000 MPa, ultimate tensile stress is 1215 MPa and 1130 MPa in the Pd–20% Ag and Pd–40% Ag alloys, respectively, which is 60% higher than these values in pure Pd (628 and 760). Simultaneously, a notable improvement of the uniform elongation up to 5.5% (Pd–20% Ag, Pd–40% Ag), i.e. almost 2 times as compared with this value for pure Pd (3.5%) was revealed. It is proposed that the latter effect is related to the enhanced dislocation storage and strain hardening capacity in these alloys due to the decreased stacking fault energy.

(iii) Our results demonstrate that decreasing the stacking fault energy γ_{SF} leads to a notable increase of strength and ductility. We propose that this method can be used to control the mechanical properties in UFG alloys.

Acknowledgements

Funding support for this work by the Deutsche Forschungsgemeinschaft (grant FOR 714) and the Russian Foundation for Basic Research of one of the authors (R.Z. Valiev) is gratefully acknowledged.

References

[1] R.Z. Valiev, R.K. Islamgaliev, I.V. Alexandrov, Prog. Mater. Sci. 45 (2000) 103.
[2] A. Zhilyaev, T.G. Langdon, Prog. Mater. Sci. 58 (2008) 893.
[3] R.Z. Valiev, Y. Estrin, Z. Horita, T.G. Langdon, M.J. Zehetbauer, Y.T. Zhu, JOM 58 (4) (2006) 33.
[4] R.Z. Valiev, M.J. Zehetbauer, Y. Estrin, H.-W. Höppel, Yu. Ivanisenko, H. Hahn, G. Wilde, H.J. Roven, X. Sauvage, T.G. Langdon, Adv. Eng. Mater. 7 (2007) 527.
[5] R.Z. Valiev, I.P. Semenova, V.V. Latysh, H. Rack, T.C. Lowe, J. Petruzelka, L. Dluhos, D. Hrusak, J. Sochova, Adv. Eng. Mater. 10 (8) (2008) B15.
[6] Y.M. Wang, E. Ma, Acta Mater. 52 (2004) 1699.
[7] M. Dao, L. Lu, R.J. Asaro, J.T.M. De Hooson, E. Ma, Acta Mater. 55 (2007) 4041.
[8] E. Ma, JOM 4 (2006) 49.
[9] Y.H. Zhao, Y.T. Zhu, X.Z. Liao, Z. Horita, T.G. Langdon, Mater. Sci. Eng. A463 (2008) 22.
[10] Y.H. Zhao, Y.T. Zhu, X.Z. Liao, Z. Horita, T.G. Langdon, Appl. Phys. Lett. 89 (2006) 121906.
[11] I. Karakaya, W.T. Thompson, in: T.B. Massalski (Editor-in-chief), H. Okamoto, P.R. Subramanian, L. Kacprzak (Eds.). Binary Alloy Phase Diagrams, vol. 1, 2nd ed., William W. Scott, 1990, p. 72.
[12] M. Levy (Editor-in-chief), H. Bass, R. Stern (Eds.). Handbook of Elastic Properties of Solids, Liquids, and Gases, vol. 2: Elastic properties of solids: theory, elements and compounds, novel materials, technological materials, alloys, and building materials, Academic Press, 2000.
[13] S. Crampin, D.D. Vedensky, R. Monnier, Philos. Mag. A67 (1993) 1447.
[14] B.J. Kestel, Ultramicroscopy 19 (1986) 205.
[15] H. Elias, D.M. Hyde, R.L. Scheaffer, A Guide to Practical Stereology, Karger, Basel u.a., 1983.
[16] M. Ames, J. Markmann, R. Karos, A. Michels, A. Tschöpe, R. Birringer, Acta Mater. 56 (2008) 4255.
[17] B.E. Warren, X-ray Diffraction, Dover, New York, 1990.
[18] R. Birringer, M. Hoffmann, P. Zimmer, Phys. Rev. Let. 88 (20) (2002) 206104.
[19] J.M. Howe, U. Dahmen, R. Gronsky, Philos. Mag. A56 (1987) 31.
[20] R.Z. Valiev, Yu. Ivanisenko, E.E. Rauch, B. Baudelet, Acta Mater. 12 (1996) 4705.
[21] H.-J. Fecht, in: A.S. Edestein, R.C. Cammarata (Eds.), Nanomaterials: Synthesis, Properties and Application, J.W. Arrowsmith Ltd., Bristol, 1996.
[22] R. Pippan, F. Wetscher, M. Hafok, A. Vorhauer, I. Sabirov, Adv. Eng. Mater. 8 (2006) 1046.
[23] F.A. Mohammed, Acta Mater. 51 (2003) 4107.
[24] Y.H. Zhao, Y.T. Zhu, X.Z. Liao, Z. Horita, T.G. Langdon, Mater. Sci. Eng. A 410–411 (2005) 188.
[25] Y.H. Zhao, Y.T. Zhu, X.Z. Liao, Z. Horita, T.G. Langdon, Mater. Sci. Eng. A 463 (2007) 22.
[26] L. Balogh, T. Ungar, Y. Zhao, Y.T. Zhu, Z. Horita, Ch. Xu, T.G. Langdon, Acta Mater. 56 (2008) 809.
[27] G.K. Willamson, R.E. Smallmann, Philos. Mag. 1 (1956) 34.
[28] R.E. Smallman, K.H. Westmacott, Philos. Mag. 2 (1957) 669.
[29] T. Ungár, A. Borbély, Appl. Phys. Lett. 69 (1996) 3173.
[30] J.P. Hirth, J. Lothe, Theory of Dislocations, Wiley, New York, 1982, pp. 332–335.
[31] DIN EN 10002, ASTM E8/E8M-08.
[32] E.O. Hall, Proc. Phys. Soc., Lond, Sect. B 64 (1951) 747.
[33] N.J. Petch, J. Iron Steel Inst. 174 (1953) 25.
[34] G.I. Taylor, Proc. Roy. Soc. A145 (1934) 362.
[35] P. Rodriguez, R.K. Krishna, J. Inst. Met. 93 (1964) 65.